ACS APPLIED MATERIALS & INTERFACES

Research Article

www.acsami.org

TiO_2 Thin Films Prepared via Adsorptive Self-Assembly for Self-Cleaning Applications

Baojuan Xi,[†,‡] Lalit Kumar Verma,[‡] Jing Li,[†] Charanjit Singh Bhatia,[‡] Aaron James Danner,[‡] Hyunsoo Yang,[‡] and Hua Chun Zeng*[,†]

[†]Department of Chemical and Biomolecular Engineering and KAUST-NUS GCR Program and [‡]Department of Electrical and Computer Engineering, Faculty of Engineering, National University of Singapore, 10 Kent Ridge Crescent, Singapore 119260

Supporting Information

ABSTRACT: Low-cost controllable solution-based processes for preparation of titanium oxide (TiO_2) thin films are highly desirable, because of many important applications of this oxide in catalytic decomposition of volatile organic compounds, advanced oxidation processes for wastewater and bactericidal treatments, self-cleaning window glass for green intelligent buildings, dye-sensitized solar cells, solid-state semiconductor metal-oxide solar cells, self-cleaning glass for photovoltaic devices, and general heterogeneous photocatalysis for fine chemicals etc. In this work, we develop a solution-based adsorptive self-assembly approach to fabricate anatase TiO_2 thin films on different glass substrates such as simple plane glass and patterned glass at variable compositions (normal soda lime glass or solar-grade boro-float glass). By tuning the number of process cycles (i.e., adsorption-then-heating) of TiO_2 colloidal suspension, we could facilely prepare large-area TiO_2 films at a desired thickness and with uniform crystallite morphology. Moreover, our as-prepared nanostructured TiO_2 thin films on glass substrates do not cause deterioration in optical transmission of glass; instead, they improve optical performance of commercial solar cells over a wide range of incident angles of light. Our as-prepared anatase TiO_2 thin films also display superhydrophilicity and excellent photocatalytic activity for self-cleaning application. For example, our investigation of photocatalytic degradation of methyl orange indicates that these thin films are indeed highly effective, in comparison to other commercial TiO_2 thin films under identical testing conditions.

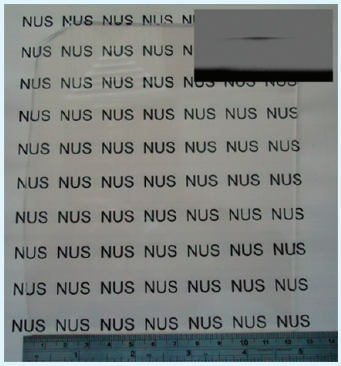

KEYWORDS: *titania, self-assembly, thin films, self-cleaning, superhydrophilicity, photocatalysis*

1. INTRODUCTION

Semiconducting metal oxides are an important class of functional materials promising a wide range of new technological applications. In particular, when prepared into thin films, the materials utilization efficiency and applicability of these materials can be significantly improved. For instance, controlled growth of titanium oxide (TiO_2) thin films on various substrates, such as glasses, polymers, silicon wafers and inorganic salts, has received increasing research attention. A great number of pioneering work has been reported over the past two decades owing to a huge commercial market of TiO_2-based products.[1−6] As a semiconducting metal oxide, TiO_2 possesses a relatively large optical band gap of 3.0−3.2 eV and is chemically stable and nontoxic. Related with its exceptional physical, electronic, photoactive, and electrochemical properties, TiO_2 holds many potential applications in the fields of solar energy conversion via solid-state or dye-sensitized solar cells,[7,8] lithium batteries or supercapacitors,[9,10] sensor applications,[11] environmental remediation including air purification,[12] wastewater treatment,[13,14] self-sterilization applications, and so on.[15] Furthermore, it was reported, in 1997, that transformation of TiO_2 films from hydrophobicity to superhydrophilicity can be achieved under the inducement of ultraviolet light.[16] This research milestone opens up a new chapter for TiO_2 applications and leads to various exploratory frontiers ranging from anti-fogging surfaces to self-cleaning surfaces.[17−20] On the basis of those reported results and documentation, intrinsic properties of TiO_2 depend largely on its structural polymorph, crystallite/grain size, terminated crystallographic planes/facets, dopants, and of course the synthetic method adopted.[21,22] In particular, anatase TiO_2 crystal phase has been considered to be superior in photocatalysis and is generally preferred to yield superhydrophilicity to rutile or anatase−rutile biphasic films.[23,24] Further to this, nanostructured TiO_2 films with a higher specific surface area can drastically enhance the photo-induced efficiency.[25,26] In this regard, therefore, preparation of TiO_2 films consisting of nanosized anatase particulate domains can be chosen as an alternative and effective avenue to improve self-cleaning performance of this transition metal oxide.

Concerning the preparation of TiO_2 films for self-cleaning application, in addition, four significant issues should be taken into account. Firstly, the TiO_2 films should have a high photocatalytic activity against common organic pollutants and a durable hydrophilicity. Secondly, the TiO_2 films should not be obviously visible on their substrates. For example, for package of silicon solar modules, the solar glass with TiO_2 coating

Received: December 6, 2011
Accepted: January 19, 2012
Published: January 19, 2012

should have high optical transmittances in order to ensure a maximum light transmission to the solar modules underneath. Thirdly, there arises another problem about the coating fabrication on arbitrarily shaped substrates for various photocatalytic reactions, especially serving for large-sized self-cleaning photovoltaic devices. And fourthly, for real practical application, the prepared TiO_2 film must adhere to its supporting substrate strongly.

Regarding the deposition of TiO_2 films onto solid substrates, two kinds of strategies can be further classified. The first one is direct nucleation of TiO_2 nuclei on a substrate surface from solution or vapor phase precursors, achieved by the classical atom-, ion-, or molecule-based nucleation and growth processes, such as sputtering,[27] spray-pyrolysis,[28] liquid phase deposition (LPD),[29] and chemical vapor deposition (CVD).[30] However, in most cases, the nucleation−growth routes likely require complicate high-cost facilities or stringent synthetic conditions involving high-temperature substrates, high vacuum/pressure, risk of residues left from the precursors, limitation of targeted materials, acceleration voltage or electrical biasing, sensitiveness to substrate surface morphology, and so on.[31−33] The second approach is to direct TiO_2-based sols or colloids onto substrate surfaces and then convert them into thin films by different kinds of post-treatments. Examples of the latter approach can be found in sol-gel thin-film processing,[34] Langmuir−Blodgett technique,[35,36] and electrophoretic deposition of nanoparticles.[37] It was reported[38] that layer-by-layer deposition of multilayers of inorganic colloidal particles, in particular, has been prevailing for TiO_2 film fabrication because of its versatility, ease of applying coating, and high quality of film thickness control.[39−41] Because separate process operations can be well-controlled, the second approach is also applied extensively for the film production. However, because of space constraints of the required equipment such as spin-coater and electrophoretic pool, the substrates and thus the TiO_2 films cannot be expanded arbitrarily and at most reach the equipment-equivalent size. Moreover, for those traditional routes like the sol−gel process, such things are also problematic as the long aging time to get workable sol, instability of precursor sol stock, and shrinkage or crack of film.[42−44] Last but not least, another obstacle is the weak adhesion between film and substrates always harassing the low temperature method including liquid phase process and they are not available for the practical application. In spite of great efforts to the TiO_2 film fabrication, some barriers are still on the way to design and synthesize TiO_2 films for advanced applications because of the complicate dependency of material properties on surface structures and synthetic routes. To meet all the three requirements imposed, a more robust cost-effective method should be developed. In this investigation, we devise a new kind of adsorptive self-assembly approach for preparation of highly transparent nanosized anatase crack-free TiO_2 thin films with good adhesion to glass substrates.

Briefly, the present approach involves three major steps: synthesis of TiO_2 colloidal nanoparticles, adsorptive self-assembly in the colloidal stock, and post-deposition heat-treatment. As depicted in Figure 1, TiO_2 nanoparticles capped with oleic acid molecules can adsorb and self-assemble on the substrate surface. After calcination, TiO_2 films can adhere more firmly to glass substrates. The thickness of TiO_2 film can be controlled precisely by the number of adsorption−heating process cycles. It should be mentioned that the starting colloidal TiO_2 particles used are only sub-10 nm in size and the fabricated TiO_2 films on glass substrates have high transmittance almost identical to

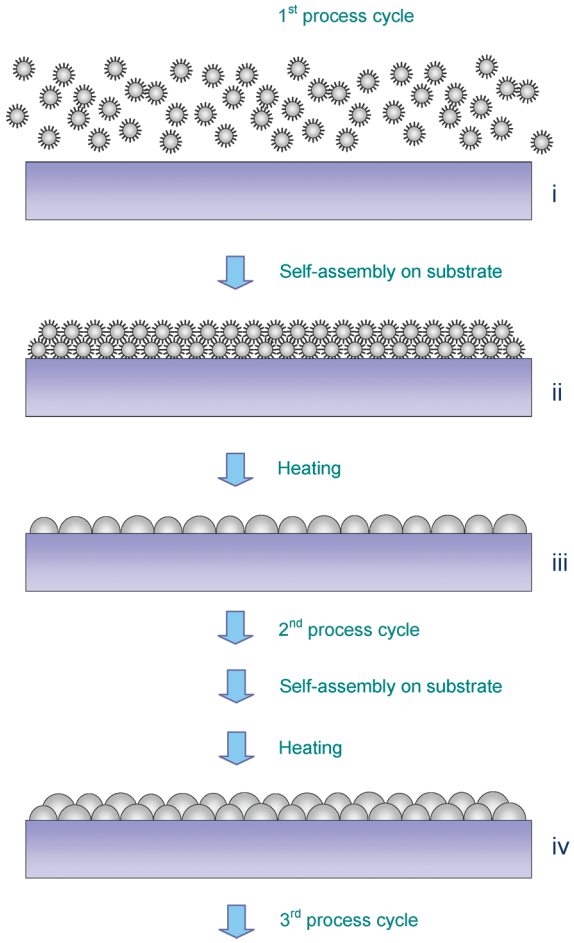

Figure 1. Process cycles (cross-sectional view) of adsorptive self-assembly of functional nanoparticles into a film on substrates: (i) functional nanoparticles suspension (e.g., oleic acid-capped TiO_2 nanoparticles), (ii) adsorption of oleic acid-capped TiO_2 nanoparticles via self-assembly on substrates, (iii) removal of capping organic surfactant (i.e., oleic acid) and growth of TiO_2 thin film on the substrates, and (iv) growth of a thicker TiO_2 film on the substrate formed in step (iii) after another adsorption-heating process cycle (i.e., the 2nd process cycle). Repeated procedures such as the 3rd and 4th process cycles can also be carried out.

the pristine bare glass. The TiO_2 suspension is very easy to obtain by dissolving the TiO_2 nanoparticles into toluene within 1 min. The suspension is very stable and can be stored for several months without any change. The solvent (toluene) used in this process can be recycled from the residual suspension by evaporation via rotor evaporator. In comparison to some representative commercial TiO_2 films, moreover, our TiO_2 films offer much higher photocatalytic activity for photo-decomposition of methyl orange under the same ambient testing conditions. On virtue of the separable and easily handled process steps involved in the fabrication, we believe that this approach can be facilely extended to other thin film preparations of metal-oxides. Because of no involvement of high cost processing equipment and adequate controllability over the product quality, scale-up for large-area thin films could be further obtained.

2. EXPERIMENTAL SECTION

2.1. Preparation of TiO_2 Colloidal Particles. Monodisperse TiO_2 nanoparticles were synthesized based on a modified experimental procedure.[45−48] Briefly, 0.20 g of titanium(IV) *n*-propoxide (98%,

Alfa Aesar) was added into 10.0 mL of toluene (AR, Aldrich). Then 6.0 mL of oleic acid (OA, $CH_3(CH_2)_7CH{=}CH(CH_2)_7COOH$, 90%, Aldrich) was added into the above mixture. A second solution containing 0.10 mL of tert-butylamine (98%, Aldrich) and 10.0 mL of deionized water was also prepared. The above two solutions were mixed and magnetically stirred for 15 min and then transferred into a Teflon-lined stainless steel autoclave. The solvothermal reaction was performed in an electric oven which had already been heated to 180 °C for a period of 7−12 h. After the synthesis, the product mixture was separated into oil and water phases. The oil phase was taken out and added with an equivalent volume of ethanol in order to precipitate TiO_2 nanoparticles. After centrifuging, the solvent was decanted and OA-capped TiO_2 nanoparticles were redispersed in 16.0 mL of toluene as a colloidal TiO_2 suspension. The concentration of TiO_2 nanoparticles in the thus prepared suspension was about 3.5 mg/mL.

2.2. Fabrication of TiO_2 Film on Glass Substrates. Soda lime glass substrates (1.5 cm ×2.5 cm ×1.0−1.2 mm; Sail brand, China) were cleaned in a Piranha solution (Caution: Piranha solution is very dangerous and has very strong oxidative ability so it should be handled carefully!)[49] which was prepared by mixing sulfuric acid (H_2SO_4, 95−97%, Merck) and hydrogen peroxide (H_2O_2, 30%, Merck) in a volume ratio of 3:1. After cleaning treatment, glass substrates were dipped in the TiO_2 colloidal suspension for 2 h to adsorb the TiO_2 nanoparticles. Samples were taken out of the suspension and washed with toluene, followed by 2 h of heat-treatment in an electric furnace at 400 °C in laboratory air. This combined soaking for 2 h and heating for 2 h is called one process cycle in our discussion. Different TiO_2 films could be fabricated by repeating this process cycle, that is, by soaking every time in a freshly prepared TiO_2 colloidal suspension followed by annealing in the laboratory air. Except the special illustration in the text, the size of glass substrates was all set at 1.5 cm × 2.5 cm × 1.0−1.2 mm. Herein, it should be mentioned that the TiO_2 suspensions could be held in either glass or plastic bottles. Therefore, TiO_2 nanoparticles would also adsorb on the wall of glass bottles, though this could be avoided by using plastic bottles. Nonetheless, for the reported data in this paper, glass bottles were exclusively used.

Nanostructured substrates (etched with inductively coupled plasma (ICP)) as well as plane substrates using borofloat glass (borofloat glass 33; Schott AG) were also investigated in this work, in order to show the conformal coatings over sub-100 nm antireflective nanostructures of solar packaging glasses.

To reduce the process cost, solvent (toluene) recovery test was performed with standard laboratory distillation method (i.e., using a simple rotary evaporator), and the purity of the recycled solvent was by analyzed by gas chromatography (GC, Agilent-7890A). Purity as high as >98% of toluene could be achieved just with a single run of distillation.

2.3. Materials Characterization. The size and crystalline structure of colloidal TiO_2 nanoparticles were investigated by transmission electron microscopy (TEM, JEM-2010, accelerating voltage: 200 kV). Structural and morphological profiles of studied samples were carried out with field emission scanning electron microscopy (FESEM, JSM-6700F, accelerating voltage: 5 kV, current: 10 μA) and atomic force microscopy (AFM, DI Nanoscope Multimode). When detected by FESEM equipment, all the samples are coated with Pt at 10 mA for 40 s. For the titania films on glass substrates, the surface and bulk chemical compositions of TiO_2 films were analyzed with energy-dispersive X-ray spectroscopy (EDX/FESEM, JEM-6700F, accelerating voltage: 15 kV, working distance: 15 mm) and X-ray photoelectron spectroscopy (XPS, AXIS-HSi, Kratos Analytical) respectively. The working pressure of XPS detection is 5×10^{-9} Torr and the X-ray source is monochromatic Al K_α ($h\nu$ = 1486.71 eV, 5 mA, 15 kV). UV−vis absorption spectra were recorded at different reaction intervals to monitor photocatalytic reactions (section 2.4) using an UV/vis spectrophotometer (Shimadzu UV-2450). The hydrophilic properties of the grown TiO_2 films were examined from a static contact angle (CA) measurement (VCA optima surface analysis system) at room temperature using a water droplet with a volume of about 1 μL.

2.4. Photocatalytic Measurements. The photocatalytic investigation for the glass supported TiO_2 films was carried out with a reference reaction of decomposition of methyl orange ($C_{14}H_{14}N_3NaO_3S$, Merck) in laboratory air at room temperature (25 °C) and under ambient pressure. The photocatalytic activity of TiO_2 films was evaluated in two different ways. Firstly, a cylindrical wide-mouth glass bottle (capacity ca. 30 mL) was used as the reactor vessel. The glass supported TiO_2 film (area at 1.5 cm × 2.5 cm) was dipped in 4.0 mL of aqueous methyl orange solution with the concentration of 5.0 mg/L and then exposed to ultraviolet (UV) light using a high-pressure mercury lamp (125 W, Philips). A cutoff filter (wavelength of 385 nm) was placed in front of the lamp which removed all emission lines of wavelength less than 385 nm. For a comparison, a control experiment was also conducted without inserting any TiO_2 film catalysts to detect the natural photodecomposition of methyl orange with the same ultraviolet irradiation. UV-vis absorption spectra of methyl orange were recorded at constant intervals to monitor the progress of photocatalytic reactions, as described in section 2.3. The second way to study the photocatalytic performance of our TiO_2 films was designed to simulate the real working condition of TiO_2 films on glass when used as the commercial self-cleaning materials under dry conditions (i.e., outside the solution). Namely, the TiO_2 film counterparts were firstly immersed in 8.0 mL of methyl orange solution at a high concentration of 250 mg/L for 2 h. After this organic deposition, the samples with the dye molecules on their surfaces were taken out and dried in the electric oven; they were then exposed vertically to the same set of the UV light source and cutoff filter. The gradual degradation of this surface organic deposit was also sequentially recorded.

2.5. Scratch Test. Scratch tests using diamond indenter were performed on as-prepared TiO_2 films to analyze the compactness and adherence of the films to the glass substrates. The radius of diamond ball used to make scratch was 1 μm, which resulted in a pressure of 1.06 GPa at an applied load of 100 mN. Although this kind of pressure is not possible in real world outdoor applications, we can estimate the film strength under extreme conditions using the test. The load was varied progressively from 0.03 to 100 mN over a distance of 1 mm. Frictional force and scratch depths were measured during the measurement and compared with uncoated glass substrates; the surface topography of the films after scratch tests was examined with atomic force microscopy (SPM, Veeco Dimension 3100).

3. RESULTS AND DISCUSSION

3.1. TiO_2 Thin Films on Plane Glass Substrates. Figure 2 gives two TEM images of the TiO_2 colloidal particles which

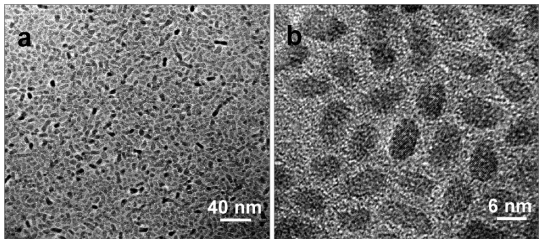

Figure 2. (a, b) TEM images of colloidal TiO_2 nanoparticles at different magnifications.

were used as starting building blocks in our self-assembled film preparation. The oxide nanoparticles show a narrow size distribution of 5−9 nm. A higher-resolution TEM image of Figure 2b indicates TiO_2 nanocrystals with clearly resolved lattice spacing of 0.352 nm, corresponding to the interspacing of (101) planes of anatase TiO_2 (see circled particles). The above analyses and results affirm that the TiO_2 nanoparticles are single-crystalline in the anatase phase. Figure 3 presents the representative surface morphology of as-synthesized TiO_2 films, showing a uniform film spreading on the glass substrate. After the first process cycle, TiO_2 nanoparticles self-assembled evenly and formed a continuous dense film on the glass surface, as

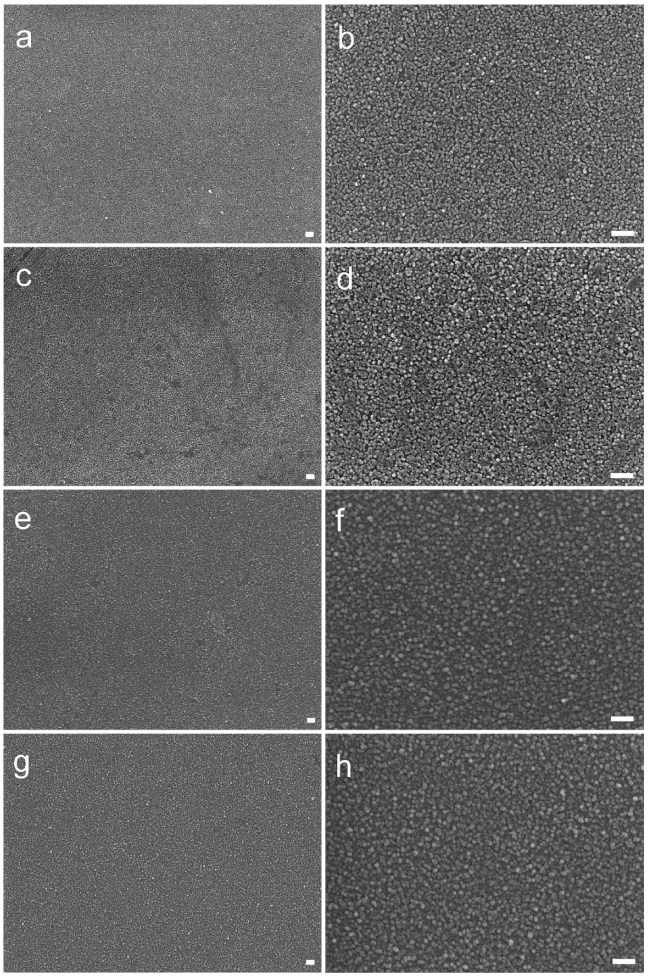

Figure 3. FESEM images of TiO_2 films on soda lime glass substrates viewed from the top at different magnifications (all scale bars in these images denoting 100 nm): (a, b) 1 process cycle (S1), (c, d) 2 process cycles (S2), (e, f) 3 process cycles (S3), and (g, h) 4 process cycles (S4).

shown in the panoramic view of Figure 3a. Through analyzing the FESEM image of Figure 3b, we find that the surface TiO_2 particles have the average size of 20 nm after heating, which were grown bigger compared to their pristine TiO_2 counterpart (i.e., the initial colloidal particles in Figure 2 and in Figure S1a,b, supporting information). At the same time, partial fusion of TiO_2 nanoparticles also took place, because nanoparticles aggregated into bigger crystal grains and interstitial voids were formed after the thermal treatment (Figure 3a,b versus Figure S1a,b, Supporting Information). Through repeated process cycles in TiO_2 suspensions, thicker TiO_2 films could be deposited on the glass surface in a stepwise fashion, as demonstrated in Figure 3c-h. Using AFM technique to characterize these films, in Figure 4, the surface of the TiO_2 films were composed of tiny grains and their average roughness was about 1.7 nm for S1 and S2 samples. With the increase in process cycles, the films became somewhat rougher but still without cracking and the average roughness reached around 2.0 nm. Because the phase-transformation from anatase to rutile takes place at a much higher temperature,[50] our TiO_2 films annealed at 400 °C remain in the anatase phase. Nevertheless, it should be pointed out that without this heat-treatment, the as-adsorbed TiO_2 nanoparticles can be removed from glass easily because of the lack of adequate chemical bonding with the substrate surface. At the same time, a pronounced peak at 285.6 eV in C 1s photoelectron spectrum of these TiO_2 films before heat-treatment can be attributed to defect-containing sp^2 hybridized carbon (see our XPS analysis in Figure S1c in the Supporting Information),[46,51] confirming the existence of OA capping molecules before calcination. During the formation of TiO_2 nanoparticles, tert-butlyamine mainly serves as an organic base to neutralize the OA and thus generates the carboxylic group which can bind on the surface of TiO_2 nuclei. After heating at 400°C for 2 h, the peak corresponding to the sp^2 hybridized carbon disappears completely (Figure S1d, Supporting Information and more XPS results will be presented in Figure 6), revealing the complete removal/decomposition of the OA molecules.[52,53] Clearly, calcination process can bring about better engagement between the TiO_2 films and glass substrates, enhancing the film adhesion and mechanical performance. Consistently, the water contact angle of TiO_2 film prior to the heat-treatment was found as high as ∼70° (see the inset photo of Figure S1a in the Supporting Information), implicating also the presence of hydrophobic OA molecules in the films and the pivotal role of thermal treatment to form the TiO_2 coating.

Table 1 summarizes the EDX results and film thickness (determined together with FESEM technique) for the samples shown in Figure 3. As expected, the progressive increase in Ti/Si atomic ratio and film thickness in these TiO_2/SiO_2 samples is in good agreement with our repeated soaking−heating cycles. Judging from the data of Table 1 and the size of pristine TiO_2 nanoparticles (Figure 2b), after the each process cycle, film must be consisted of about 10−15 layers of adsorbed TiO_2 nanoparticles. In addition, the TiO_2 films prepared with one to four process cycles are all absolutely clear and transparent and have a light transmittance nearly the same as their pristine bare glass substrates, as reported in Figure 5a with the normal incidence of light. In fact, most samples show overlapping transmission curves, suggesting their suitability of solar cell applications. Furthermore, the freshly prepared samples exhibit excellent superhydrophilic nature with a water contact angle of ∼0° (the photograph in the inset of Figure 5a) and still retained at ∼15° even though they were kept in dark for a week. In order to investigate their applicability for self-cleaning solar cells, we also measured the transmitting property of these films with all-directional incident light. Figure 5b gives the transmittance curves versus the incident light at the wavelength of 400 nm. By comparing with the uncoated glass, we find that these self-assembled TiO_2 films indeed show a good all-dimensional transmittance close to their original glass substrate.

To further demonstrate the versatility of this adsorptive self-assembly route, we have also conducted a series of related experiments. For example, the soda lime glass substrates were replaced with borofloat glass (borofloat glass 33; Schott AG) to see the reproducibility of film formation. As expected, very uniform thin films of TiO_2 on the borofloat glass can also be obtained (see FESEM results, Figure S2 in the Supporting Information) using the same synthetic procedures adopted in Figure 3. However, aggregated crystal particles consisting of these films have a larger size distribution in the range of 9−18 nm compared to those formed on the soda lime glass in Figure 3. Apart from the crystallite size variation, the films are also highly transparent. Similarly, the water contact angle on the borofloat glass decreased from 60° to ∼1° after the formation of

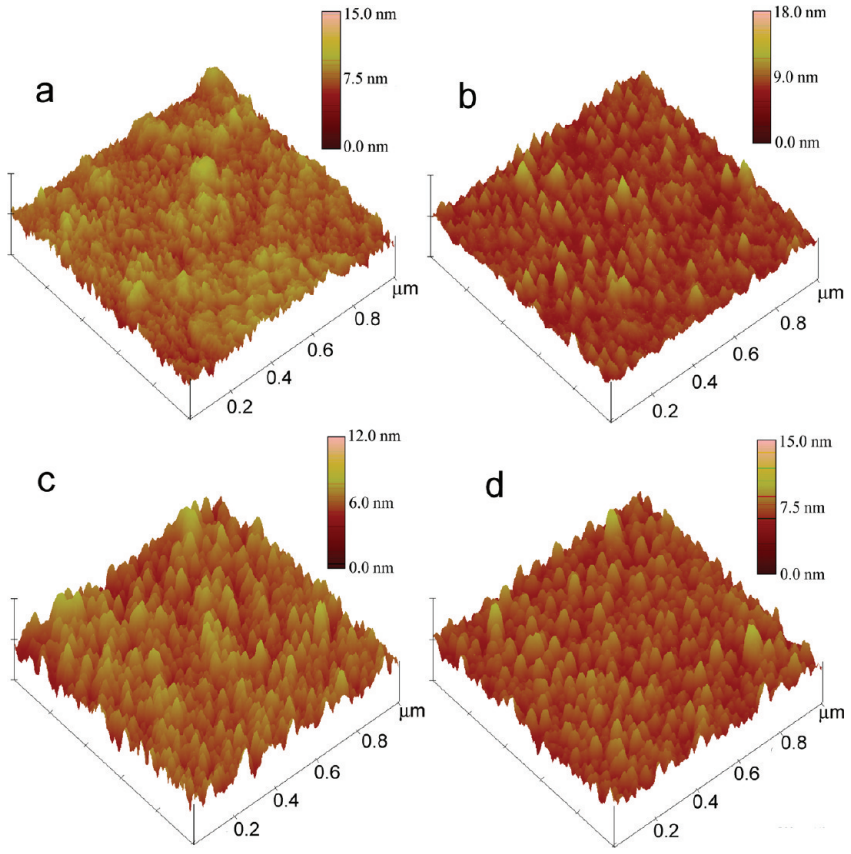

Figure 4. Representative AFM images indicating the surface topographies of (a) 1 process cycle (S1), (b) 2 process cycles (S2), (c) 3 process cycles (S3), and (d) 4 process cycles (S4).

Table 1. Summary of EDX Results and Thickness of TiO_2 Thin Films Shown in Figure 3

sample	number of process cycle	accumulative soaking duration (h)	Ti/Si atomic ratio from EDX	film thickness (nm)
S1	1	2	0.0003	70 ± 4
S2	2	2 + 2	0.0015	209 ± 8
S3	3	2 + 2 + 2	0.0026	340 ± 12
S4	4	2 + 2 + 2 + 2	0.0049	460 ± 14

the TiO_2 films, demonstrating the as-formed TiO_2 films are also superhydrophilic.

3.2. TiO_2 Thin Films on Patterned Glass Substrates. Beause infantile TiO_2 particles were very small in size, they likely could adsorb and thus spread over to the every point of a substrate. In order to verify this postulation, the same filming process was extended to nanostructured glass, according to a flowchart (see Figure S3 in the Supporting Information). We etched the borofloat glass substrate with inductively coupled plasma (ICP) and obtained two kinds of nanostructures with pillar- and holed patterns. As is expected, FESEM study of Figure 6 reveals resultant topographical surface nanostructures, whose elemental EDX analysis can be found in Figure S4 (Supporting Information), testifying the formations of TiO_2 films both on the pillar-patterned glass and hole-patterned glass. The transmittance reported in Figure 6e decreases little in contrast with the bare borofloat glass, and at the same time, the reducing water contact angle from ~37° to below 10° (Figure 6f) further confirms the growth of TiO_2 film on holed glass. The above results suggest that TiO_2 nanocrystals could self-assemble uniformly on different kinds of patterned glass surfaces.

As mentioned earlier, this adsorptive self-assembly method does not involve any complicated process or sophisticated apparatus and, in principle, preparation of larger area thin films of TiO_2 should be achievable. To test out this point further, we also carried out some preliminary scale-up experiments using the process parameters acquired in the above studies. For example, we used a larger piece of borofloat glass plate at the size of 12.5 cm × 12.5 cm ×2.0 mm and dipped it in 350 mL of TiO_2 suspension for a soaking (adsorption) period of 2 h, followed by the same annealing treatment at 400°C for 2 h. Surface morphology of this TiO_2 film is very flat with a high light transmittance and a small water contact angle below 10° (see Figure S5 in the Supporting Information). This experiment indeed illustrates the scalability of the present method. We further investigated the recovery of major solvent toluene using a simple evaporation−condensation method. The purity of obtained toluene was as high as 98% (determined by GC) by just one run of distillation treatment.

3.3. Surface Analysis and Adsorptive Self-Assembly. To get more information about the surface and chemical composition of constituent elements in these films, a comparative XPS analysis was conducted for samples fabricated both on the soda lime glass and borofloat glass. In Figure 7, the binding energies (BEs) of XPS spectra of all studied elements are referred to C 1s photoelectron peak originating from adventitious carbon (its BE was set at 284.6 eV);[46,54] other two weak C 1s peaks located at 286.0−286.2 and 288.2−288.3 eV are assigned to hydroxyl carbon (HO−C) and carboxylate/carbonate

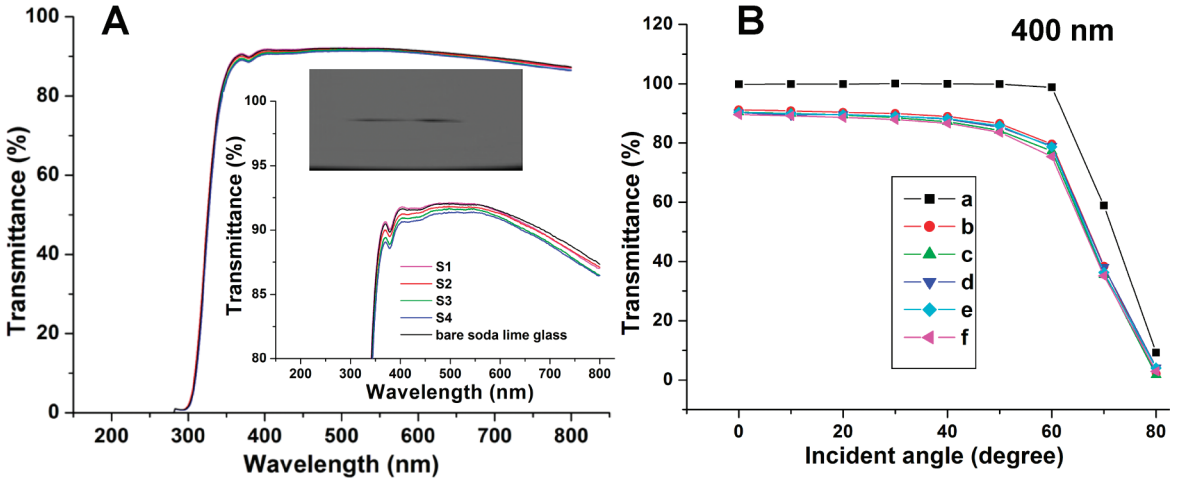

Figure 5. (A) Optical transmittance of samples S1, S2, S3, and S4 (Figure 3); inset shows higher-resolution transmittance spectra with the normal incidence. Water contact angle image reveals the superhydrophilic nature of freshly prepared TiO_2 films. (B) Optical transmittance of samples versus varied incident angles of light at the wavelength of 400 nm: (a) equipment reference, (b) bare soda lime glass, (c) S1, (d) S2, (e) S3, and (f) S4.

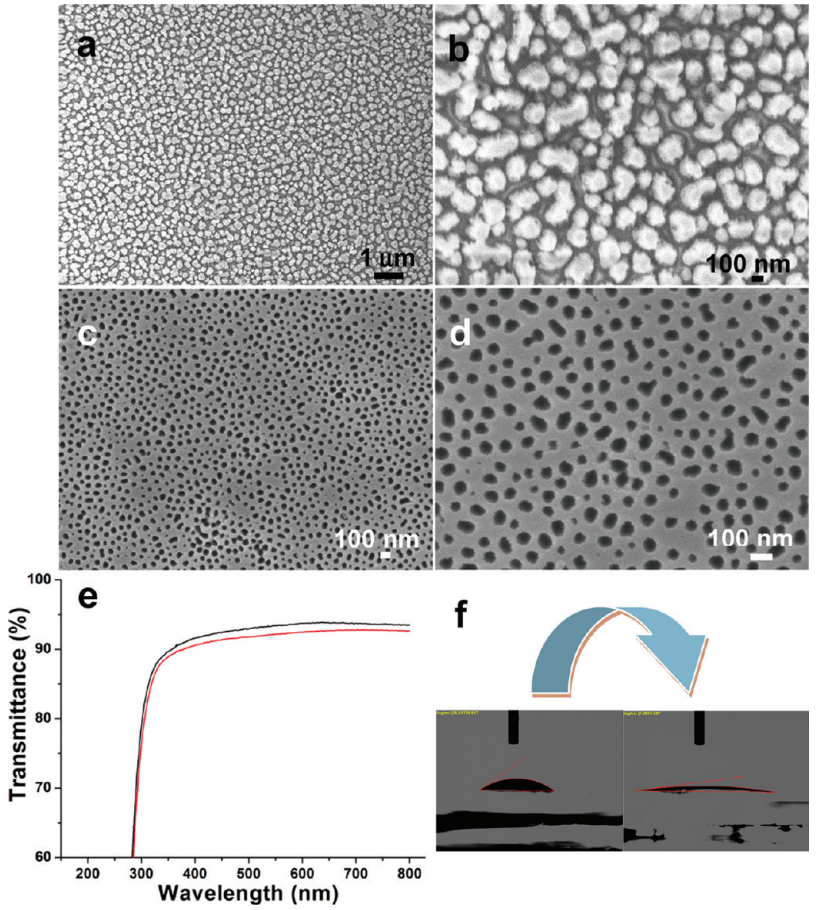

Figure 6. (a, b) FESEM images of a TiO_2 film formed on pillar-patterned borofloat glass at different magnifications, (c, d) FESEM images of a TiO_2 film grown on the hole-patterned borofloat glass at different magnifications; (e) transmittance spectra; black and red curves were measured for hole-patterned borofloat glass before and after formation of the TiO_2 film (images of c and d), respectively; and (f) water contact angle photos of hole-patterned glass before and after formation of the TiO_2 film (images of c and d).

anions,[46,47,55] respectively. All O 1s spectra can be deconvoluted into four peaks. The two identical peaks at 532.7 eV are due to the bridging oxygen in Si−O−Si,[56−58] namely, the main component of glass. The other peaks at 530.9, 531.4−531.8, and 533.2 eV are attributed to adsorbed hydroxyl (−OH), and Si−O−Ti/M (M denoting other metal elements contained in glass)[48,56,58,59] and water molecules,[46,48] respectively, suggesting the presence of a hydrophilic surface. The peaks at 529.5−529.8 eV are commonly assigned to the lattice oxygen of anatase phase. In this agreement, the doublet peaks of Ti 2p photoelectrons at 458.1−458.5 eV and 463.9−464.3 eV further confirm the presence of anatase phase before and after

dx.doi.org/10.1021/am201721e | ACS Appl. Mater. Interfaces 2012, 4, 1093−1102

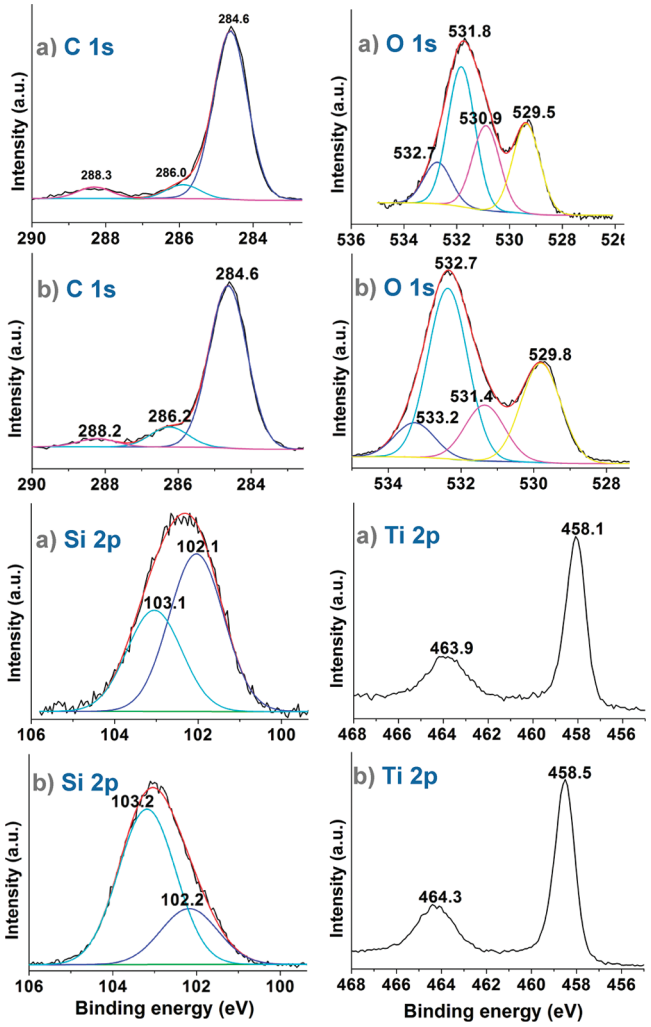

Figure 7. XPS spectra of C 1s, O 1s, Si 2p, and Ti 2p photoelectrons of (a) TiO_2 film on soda lime glass substrate, and (b) TiO_2 film on borofloat glass substrate.

calcination on the both glass substrates.[46,48,60,61] As for the Si 2p photoelectrons, the two peaks at 103.1−103.2 eV and 102.1−102.2 eV are ascribed to Si elements of the above-mentioned Si−O−Si and Si−O−Ti/M linkages.[59]

The interaction between colloidal TiO_2 and glass substrates should be further addressed. Generally, the layer-by-layer deposition depends on the electrostatic interaction between the nanoparticles from suspensions and substrates with opposite charges.[38] To have some insights on this, we also used soda lime glass without cleaning with Piranha process for TiO_2 deposition. In such a case, formation of isolated TiO_2 islands on the glass substrates was found (FESEM result, see Figure S6 in the Supporting Information), suggesting that TiO_2 can only be added to certain locations of the glass substrate, and attractive electrostatic force of opposite charges is unlikely to be a major cause for the adsorption because the OA-capped TiO_2 nanoparticles are not charged. We further examined the effect of adsorption time on the formation of TiO_2 thin films. As shown in Figure 8, the initial yellowish transparent TiO_2 colloidal suspension turned white turbid when the soaking duration of glass was beyond 12 days, and white precipitates could then be seen at the bottle bottom after 18 days. This observation indicates that TiO_2 nanoparticles became less protected by the oleic

Figure 8. TiO_2 colloidal suspension changed with the soaking time: (i) 0 day, (ii) 12 days, and (iii) 18 days. Note that the glass substrates were transferred out of the solution during the photo-taking.

acid (OA) capping after the prolonged standing in toluene. Consistent with this postulation (and unlike those shown in Figure 2), the TiO_2 nanoparticles after soaking for 18 days were are indeed more aggregative with a reduction in inter-crystal space, and direct contact among the nanocrystals could be observed (see the Supporting Information, Figure S7). Because we did not observe any aggregation among the TiO_2 colloidal nanocrystals in our normal coating operation (i.e., within hours, which was much shorter than 12 days), the adsorption due to van der Waals interaction among the surface OA molecules can be ruled out. On the other hand, we observed the adsorption of the as-prepared TiO_2 nanoparticles took place readily on the cleaned glass substrate even within 10 seconds (see Figure S8 in the Supporting Information), which indicated there must be a partial disengagement of OA-capping from the TiO_2 nanoparticles in order to generate aggregative thin films of the nanoparticles, because unprotected TiO_2 nanoparticles would be very reactive. Therefore, we propose the following self-assembly mechanism. During the initial adsorption, the OA surfactant was partially disengaged and surface hydroxyl groups of TiO_2 nanoparticles would react with those of silica substrate, forming Ti−O−Si linkages (i.e., Ti−OH + HO−Si → Ti−O−Si + H_2O). Afterwards, the assembly mainly took place among the TiO_2 nanoparticles. In particular, the OA surfactant must also be partially removed and surface hydroxyl groups of incoming TiO_2 nanoparticles would then react with the hydroxyl groups of previously deposited TiO_2 nanoparticles, resulting in formation of Ti−O−Ti bonding (Ti−OH + HO−Ti → Ti−O−Ti + H_2O) or direct contact among the TiO_2 nanoparticles. This adsorptive self-assembly would go on and the thickness of the TiO_2 nanoparticle film depended on the length of process time. Similar explanation can also be given to the second, the third, and their following process cycles.

In the above proposed mechanism, surface hydroxyl groups of silica substrate must play a crucial role to initiate the TiO_2 adsorption. This is consistent with our observations made with untreated and treated glass substrates. Without cleaning (see Figure S6 in the Supporting Information), surface active sites for adsorption were limited (because of a layer of pristine grease/stains) that largely depends on opposite charges provided by the nanoparticles and poly-electrolytes used in the film fabrications.[39−41] After cleaned with Piranha process, however, the soda lime glass substrates exhibited high hydrophilicity, indicating the presence of abundant surface −OH groups (also consistent with the XPS results in Figure 7). In this regard, the surface cleaning would ensure an even deposition of the TiO_2 nanoparticles onto the SiO_2 substrate as well as the subsequent TiO_2 to TiO_2 deposition. Apparently, the present adsorptive self-assembly process is different from the reported layer-by-layer deposition of TiO_2 colloidal nanoparticles.

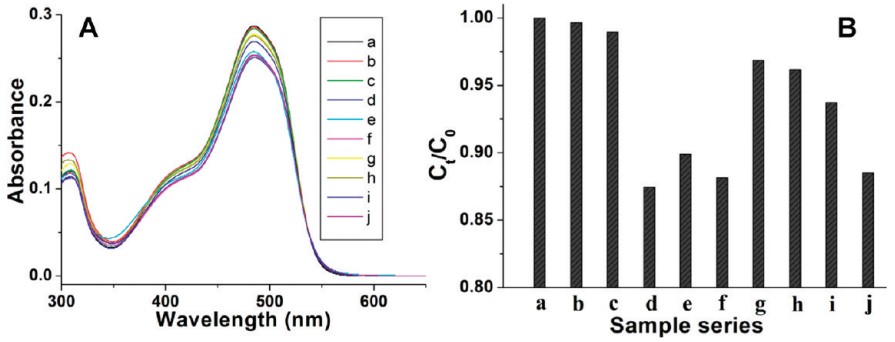

Figure 9. (A) Absorption spectra of methyl orange solution (5 mg/L, 4 mL) without and with various TiO_2 films on soda lime glass substrates under exposure to the UV light lamp for 6 h: (a) initial methyl orange solution, (b) without any catalyst, (c) S1 (prepared by 1 process cycle), (d) S2 (by 2 process cycles), (e) S3 (by 3 process cycles), (f) S4 (by 4 process cycles), (g) sample prepared in the same way as S1 but with a soaking time of 4 h, (h) sample prepared in the same way as S1 but with a soaking time of 6 h, (i) sample prepared in the same way as S1 but with a soaking time of 8 h, (j) sample prepared in the same way as S1 but with a soaking time of 12 days; and (B) the corresponding C_t/C_0 plot versus the sample series.

3.4. Self-Cleaning Application. To demonstrate the potential self-cleaning applicability, the photocatalytic behavior of the as-prepared films was investigated using the photocatalytic degradation of methyl orange as a model reaction, during which the characteristic absorption of this dye molecule at ca. 485 nm was used to monitor its degradation process. Furthermore, to verify the effectiveness of the present adsorptive assembling route, we also prepared several batches of TiO_2 film samples with a deposition time varying from 4 to 8 h. Figure 9A displays a series of absorption spectra of methyl orange aqueous solution (initial concentration of 5.0 mg/L) measured for this degradation reaction in absence of a catalyst or in presence of various TiO_2 films. All the sample films reported were exposed to an UV irradiation (UV lamp, 125 W; see Experimental Section) for 6 h, and their corresponding C_t/C_0 data after the exposure to the UV light are also plotted in this Figure. It is found that S2, S3 and S4 films all have a higher photocatalytic activity compared to their counterpart samples (i.e., samples g to i, Figure 9B) prepared with the same total soaking times of 4, 6, and 8 h, respectively. When the soaking time was extended to 12 days, the resultant TiO_2 film (sample j, Figure 9B) still shows a lower activity than S2, which further justifies the effectiveness of this multiple-coating route to prepare TiO_2 films. It can be noticed that the TiO_2 film prepared with two process cycles (S2) has a superior photocatalytic performance to other samples with one, three or four process cycles (Figure 9). When only one process cycle of TiO_2 was deposited on the glass substrate (i.e., S1), the film is too thin to have good photocatalytic activity. After the two process cycles, the quantity of TiO_2 film (S2) as well as the total surface area increases because of the rise of existing interparticle space. With more deposited layers, the TiO_2 phase definitely grows in quantity, but the photocatalytic efficiency instead declines, which could be attributed to a significant crystallite coarsening among the TiO_2 nanoparticles when the overall thickness of the films increases.

To understand the potential advantage of these films in self-cleaning application, we also immersed the soda lime glass supported TiO_2 films in 8.0 mL of 250 mg/L of methyl orange solution for 2 h to disseminate methyl orange on the surface and compared its efficiency with commercial TiO_2 films (spray coated samples, proprietary source information; samples supplied by Haruna, Singapore) under the identical reaction conditions. Time-dependent $\ln C_t/C_0$ curves of residual methyl orange are recorded (see the Supporting Information, Figure S9,) and once again it is found that the sample prepared with two process cycles has the best photocatalytic activity and is much more efficient than the commercial TiO_2 films fabricated via three spray process cycles of commercial titania powder, which may be attributable to much smaller grain size and special nanostructure of the TiO_2 films prepared with our approach, in comparison to those in the commercial products (see Figure S10 in the Supporting Information).

For the practical application of these TiO_2 coatings, the mechanical durability is an important factor. In Figure 10, therefore, the normalized frictional force curves measured during scratch tests performed on several TiO_2 film samples are reported. Understandably, the oscillations of the curves manifest the formation of cracks in the film and a resultant decrease in the friction measured by the diamond ball. As the diamond ball penetrates deeper, the friction force increases again until the formation for a new crack. The uncoated glass shows formation of cracks at a force of 25−28 mN, which is delayed to higher values with each process cycle of TiO_2 growth. Samples with three process cycles shows formation of large cracks shifted to 50 mN. In practical world, a force of 5 mN is equivalent to normal hand cleaning of surfaces; hence the scratch

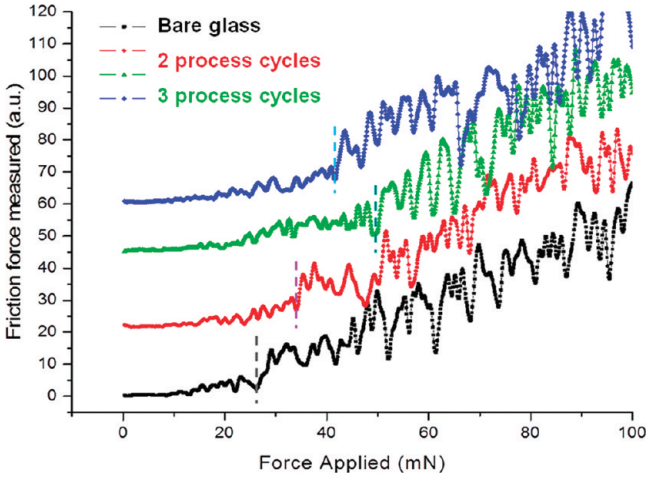

Figure 10. Frictional forces measured with a diamond tip of 1 μm diameter on soda lime glass substrates coated with the TiO_2 thin films. Plots are shifted in y-scale from each other for better clarity to the readers (the thresholds of crack formation are indicated with vertical dashed lines).

dx.doi.org/10.1021/am201721e | ACS Appl. Mater. Interfaces 2012, 4, 1093−1102

test indicates a huge increase in the life span of the module packaging. Nevertheless, thicker films show easy peeling-off and breakage of films. The atomic force micrographs in Figure 11

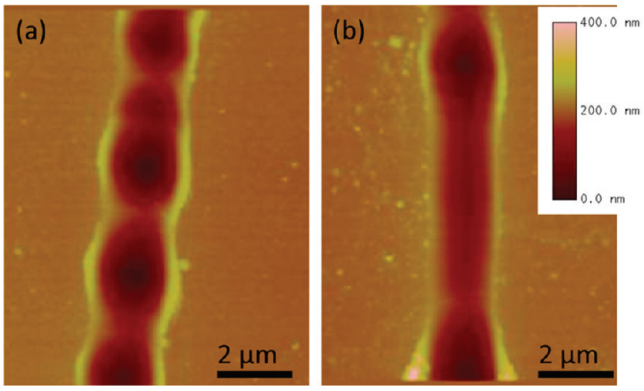

Figure 11. Atomic force microscopic images showing the surface of two TiO_2 thin films on soda lime glass after their scratch tests. The TiO_2 films shown here were prepared with (a) 3 process cycles, and (b) 4 process cycles.

present that the TiO_2 films up to three process cycles of growth adhere strongly to the substrates and offer resistance to scratches. The TiO_2 films grown with four process cycles or more break easily and show less resistance at the scratch site because nanoparticles were not adhering well with each other in a thicker film. By comparing with bare glass, the as-prepared TiO_2 films show good anti-scratching property, which suggests that our samples potentially can serve as cover glasses for self-cleaning solar panels. In fact, we are preparing TiO_2 films on large-sized glass substrates (6 × 6 square inches) now in order to cover commercial solar panels. The successful preparation of these large-sized TiO_2 films will allow us to investigate time-dependent output power efficiency and at the same time to develop the self-cleaning solar panels as well as other types of self-cleaning devices and applications.

4. CONCLUSION

In summary, in this work, we have devised an adsorptive self-assembly approach for solution-based preparation of anatase TiO_2 thin films. Using the presynthesized anatase nanoparticles as starting building blocks, high-quality TiO_2 thin films can be assembled uniformly onto various plane glass substrates, including normal soda lime glass and solar-grade borofloat glass. In addition to the variation in substrate composition, the same TiO_2 thin films can also be prepared onto nanostructure-patterned glass substrates. Because of its processing simplicity and architectural flexibility, the present synthetic strategy can be facilely employed in large-scaled TiO_2 thin film preparations and we have successfully achieved the uniform film size for the studied glass substrates from 1.5 cm × 2.5 cm × 1.0−1.2 mm to 12.5 cm × 12.5 × 2.0 mm. Our microscopic investigation demonstrates the smooth and conformal surface with no cracks, and our scratch tests suggest a good interfacial adhesion between TiO_2 films and glass substrates enhanced by the thermal post-treatment at 400 °C. Through repeated adsorption-heating process cycles, the thickness and crystallite morphology of the thin films can be further tuned. The freshly-prepared TiO_2 films has excellent super-hydrophilic surface with a water contact angle below 5° and maintain at a low contact angle of about ∼15° after stored in dark place for a week. Furthermore, the photocatalytic performance of the TiO_2 thin films fabricated by the present approach is found to be better than commercially available spray-coated TiO_2 films. Becuse of its high transmittance, therefore, our TiO_2 thin films indeed can act as omni-directional self-cleaning coating on solar panels with very little loss of power efficiency. After more future investigations, in principle, the present adsorptive self-assembly approach should also be extendable to thin film processes for other advanced functional material systems.

■ ASSOCIATED CONTENT

Ⓢ Supporting Information

FESEM and TEM images, EDX, XPS, and UV−vis results, and photocatalytic reaction data. This material is available free of charge via the Internet at http://pubs.acs.org/.

■ AUTHOR INFORMATION

Corresponding Author

*E-mail: chezhc@nus.edu.sg.

Notes

The authors declare no competing financial interest.

■ ACKNOWLEDGMENTS

This work is supported by National Research Foundation (NRF) Grant R-263-000-544-272. H.C.Z. thanks King Abdullah University of Science and Technology, Saudi Arabia, for providing financial support.

■ REFERENCES

(1) Ji, Y. J.; Lin, K.-C.; Zheng, H. G.; Liu, C.-C.; Dudik, L.; Zhu, J. J.; Burda, C. *ACS Appl. Mater. Interfaces* **2010**, *2*, 3075−3082.
(2) Kamegawa, T.; Suzuki, N.; Yamashita, H. *Energy Environ. Sci.* **2011**, *4*, 1411−1416.
(3) Takahashi, M.; Inoue, M.; Ihara, R.; Yoko, T.; Nemoto, T.; Isoda, S.; Malfatti, L.; Costacurta, S.; Innocenzi, P. *Adv. Mater.* **2010**, *22*, 3303−3306.
(4) Yu, J. G.; Dai, G. P.; Cheng, B. *J. Phys. Chem. C* **2010**, *114*, 19378−19385.
(5) Burbure, N. V.; Salvador, P. A.; Rohrer, G. S. *Chem. Mater.* **2010**, *22*, 5823−5830.
(6) Nam, S.-W.; Lee, M.-H.; Lee, S.-H.; Lee, D.-J.; Rossnagel, S. M.; Kim, K.-B. *Nano Lett.* **2010**, *10*, 3324−3329.
(7) Gao, F. F.; Wang, Y.; Shi, D.; Zhang, J.; Wang, M. K.; Jing, X. Y.; Humphry-Baker, R.; Wang, P.; Zakeeruddin, S. M.; Grätzel, M. *J. Am. Chem. Soc.* **2008**, *130*, 10720−10728.
(8) Varghese, O. K.; Paulose, M.; Grimes, C. A. *Nat. Nanotechnol.* **2009**, *4*, 592−597.
(9) Chen, J. S.; Tan, Y. L.; Li, C. M.; Cheah, Y. L.; Luan, D. Y.; Madhavi, S.; Boey, F. Y. C.; Archer, L. A.; Lou, X. W. *J. Am. Chem. Soc.* **2010**, *132*, 6124−6130.
(10) Wang, Q.; Wen, Z. H.; Li, J. H. *Adv. Funct. Mater.* **2006**, *16*, 2141−2146.
(11) Hu, P. G.; Du, G. J.; Zhou, W. J.; Cui, J. J.; Lin, J. J.; Liu, H.; Liu, D.; Wang, J. Y.; Chen, S. W. *ACS Appl. Mater. Interfaces* **2010**, *2*, 3263−3269.
(12) Fujishima, A.; Zhang, X. T.; Tryk, D. A. *Surf. Sci. Rep.* **2008**, *63*, 515−582.
(13) Mills, A.; Sheik, M.; O'Rourke, C.; McFarlane, M. *Appl. Catal. B: Environ.* **2009**, *89*, 189−195.
(14) Blanco-Galvez, J.; Fernández-Ibáñez, P.; Malato-Rodríguez, S. *J. Solar Energy Eng.* **2007**, *129*, 4−15.
(15) Hayden, S. C.; Allam, N. K.; El-Sayed, M. A. *J. Am. Chem. Soc.* **2010**, *132*, 14406−14408.
(16) (a) Wang, R.; Hashimoto, K.; Fujishima, A.; Chikuni, M.; Kojima, E.; Kitamura, A.; Shimohigoshi, M.; Watanabe, T. *Nature*

1997, *338*, 431−432. (b) Wang, R.; Hashimoto, K.; Fujishima, A.; Chikuni, M.; Kojima, E.; Kitamura, A.; Shimohigoshi, M.; Watanabe, T. *Adv. Mater.* **1998**, *10*, 135−138.
(17) Prado, R.; Beobide, G.; Marcaide, A.; Goikoetxea, J.; Aranzabe, A. *Sol. Energy Mater. Sol. Cells* **2010**, *94*, 1081−1088.
(18) Gu, Z. Z.; Fujishima, A.; Sato, O. *Appl. Phys. Lett.* **2004**, *85*, 5067−5069.
(19) Gan, W. Y.; Lam, S. W.; Chiang, K.; Amal, R.; Zhao, H. J.; Brungs, M. P. *J. Mater. Chem.* **2007**, *17*, 952−954.
(20) Zorba, V.; Chen, X. B.; Mao, S. S. *Appl. Phys. Lett.* **2010**, *96*, 093702.
(21) (a) Zhang, Z. B.; Wang, C.-C.; Zakaria, R.; Ying, J. Y. *J. Phys. Chem. B* **1998**, *102*, 10871−10878. (b) Peng, J.; Li, X.; Kim, D. H.; Knoll, W. *Macromol. Rapid Commun.* **2007**, *28*, 2055−2061.
(22) (a) Zheng, Z. K.; Huang, B. B.; Qin, X. Y.; Zhang, X. Y.; Dai, Y.; Jiang, M. H.; Wang, P.; Whangbo, M. -H. *Chem.—Eur. J.* **2009**, *15*, 12576−12579. (b) Ohno, T.; Sarukawa, K.; Tokieda, K.; Matsumura, M. *J. Catal.* **2001**, *203*, 82−86. (c) Gao, L.; Zhang, Q. H. *Scr. Mater.* **2001**, *44*, 1195−1198.
(23) Karakitsou, K. E.; Verykios, X. E. *J. Phys. Chem.* **1993**, *97*, 1184−1189.
(24) Ohno, T.; Sarukawa, K.; Matsumura, M. *J. Phys. Chem. B* **2001**, *105*, 2417−2420.
(25) Liu, G.; Sun, C. H.; Yang, H. G.; Smith, S. C.; Wang, L. Z.; Lu, G. Q.; Cheng, H. -M. *Chem. Commun.* **2010**, *46*, 755−757.
(26) Hoffmann, M. R.; Martin, S. T.; Choi, W.; Bahnemann, D. W. *Chem. Rev.* **1995**, *95*, 69−96.
(27) Awitor, K. O.; Rivaton, A.; Gardette, J.-L.; Down, A. J.; Johnson, M. B. *Thin Solid Films* **2008**, *516*, 2286−2291.
(28) Okuya, M.; Nakade, K.; Kaneko, S. *Sol. Energy Mater. Sol. Cells* **2002**, *70*, 425−435.
(29) Ding, Y. B.; Yang, C. Z.; Zhu, L. H.; Zhang, J. D. *J. Hazard. Mater.* **2010**, *175*, 96−103.
(30) Kafizas, A.; Dunnill, C. W.; Parkin, I. P. *J. Mater. Chem.* **2010**, *20*, 8336−8349.
(31) Raj, A. M. E.; Agnes, V.; Jothy, V. B.; Ravidhas, C.; Wollschläger, J.; Suendorf, M.; Neumann, M.; Jayachandran, M.; Sanjeeviraja, C. *Thin Solid Films* **2010**, *519*, 129−135.
(32) Yildirim, G.; Akdogan, M.; Varilci, A.; Terzioglu, C. *Cryst. Res. Technol.* **2010**, *45*, 1161−1165.
(33) Takeuchi, M.; Sakamoto, K.; Tsujimaru, K.; Anpo, M. *Catal. Lett.* **2009**, *131*, 189−193.
(34) (a) Pomoni, K.; Vomvas, A.; Todorova, N.; Giannakopoulou, T.; Mergia, K.; Trapalis, C. *J. Alloys Compd.* **2011**, *509*, 7253−7258. (b) Pinho, L.; Mosquera, M. J. *J. Phys. Chem. C* **2011**, *115*, 22851−22862.
(35) Natori, H.; Kobayashi, K.; Takahashi, M. *J. Oleo Sci.* **2009**, *58*, 203−211.
(36) Umemura, Y.; Shinohara, E.; Koura, A.; Nishioka, T.; Sasaki, T. *Langmuir* **2006**, *22*, 3870−3877.
(37) Moskalewicz, T.; Czyrska-Filemonowicz, A.; Boccaccini, A. R. *Surf. Coat. Technol.* **2007**, *201*, 7467−7471.
(38) Iler, R. K. *J. Colloid Interface Sci.* **1966**, *21*, 569−594.
(39) Uğur, Ş. S.; Sarıışık, M.; Aktaş, A. H. *Nanotechnology* **2010**, *21*, 325603.
(40) Habibi, M. H.; Zendehdel, M. *Curr. Nanosci.* **2010**, *6*, 642−647.
(41) Lee, D.; Omolade, D.; Cohen, R. E.; Rubner, M. F. *Chem. Mater.* **2007**, *19*, 1427−1433.
(42) Chan, C.-C.; Chang, C.-C.; Hsu, W.-C.; Wang, S.-K.; Lin, J. *Chem. Eng. J.* **2009**, *152*, 492−497.
(43) Ding, Y. B.; Yang, C. Z.; Zhu, L. H.; Zhang, J. D. *J. Hazard. Mater.* **2010**, *175*, 96−103.
(44) Deki, S.; Aoi, Y.; Hiroi, O.; Kajinami, A. *Chem. Lett.* **1996**, 433−434.
(45) Pan, D. C.; Zhao, N. N.; Wang, Q.; Jiang, S. C.; Ji, X. L.; An, L. J. *Adv. Mater.* **2005**, *17*, 1991−1995.
(46) Li, J.; Tang, S. B.; Lu, L.; Zeng, H. C. *J. Am. Chem. Soc.* **2007**, *129*, 9401−9409.
(47) Wang, D. P.; Zeng, H. C. *J. Phys. Chem. C* **2009**, *113*, 8097−8106.
(48) Wang, D. P.; Zeng, H. C. *Chem. Mater.* **2009**, *21*, 4811−4823.
(49) Kim, T.-H.; Sohn, B.-H. *Appl. Surf. Sci.* **2002**, *201*, 109−114.
(50) Sasaki, T.; Komatsu, Y.; Fujiki, Y. *Chem. Mater.* **1992**, *4*, 894−899.
(51) Lee, K. Y.; Kim, M.; Hahn, J.; Suh, J. S.; Lee, I.; Kim, K.; Han, S. W. *Langmuir* **2006**, *22*, 1817−1821.
(52) Limaye, M. V.; Singh, S. B.; Date, S. K.; Kothari, D.; Reddy, V. R.; Gupta, A.; Sathe, V.; Choudhary, R. J.; Kulkarni, S. K. *J. Phys. Chem. B* **2009**, *113*, 9070−9076.
(53) Ayyappan, S.; Gnanaprakash, G.; Panneerselvam, G.; Antony, M. P.; Philip, J. *J. Phys. Chem. C* **2008**, *112*, 18376−18383.
(54) Li, J.; Zeng, H. C. *Angew. Chem. Int. Ed.* **2005**, *44*, 4342−4345.
(55) Kovtyukhova, N. I.; Mallouk, T. E.; Pan, L.; Dickey, E. C. *J. Am. Chem. Soc.* **2003**, *125*, 9761−9769.
(56) Teo, S. H.; Zeng, H. C. *J. Phys. Chem. B* **2001**, *105*, 9093−9100.
(57) Iwamoto, S.; Iwamoto, S.; Inoue, M. *Chem. Mater.* **2005**, *17*, 650−655.
(58) Xie, C.; Yang, Q. J.; Xu, Z. L.; Liu, X. J.; Du, Y. G. *J. Phys. Chem. B* **2006**, *110*, 8587−8592.
(59) Zhang, X.; Zhang, F.; Chan, K. -Y. *Appl. Catal. A* **2005**, *284*, 193−198.
(60) Cebeci, F. Ç.; Wu, Z. Z.; Zhai, L.; Cohen, R. E.; Rubner, M. F. *Langmuir* **2006**, *22*, 2856−2862.
(61) Li, F. B.; Li, X. *Z. Appl. Catal. A* **2002**, *228*, 15−27.